



HHS Public Access

Author manuscript

Environ Sci Technol. Author manuscript; available in PMC 2021 November 03.

Published in final edited form as:

Environ Sci Technol. 2020 November 03; 54(21): 13439–13447. doi:10.1021/acs.est.0c03761.

Estimating Wildfire Smoke Concentrations During the October 2017 California Fires Through BME Space/Time Data Fusion of Observed, Modeled, and Satellite-Derived PM_{2.5}

Stephanie E. Cleland[†], J. Jason West[†], Yiqin Jia[‡], Stephen Reid[‡], Sean Raffuse[§], Susan O'Neill^{||}, Marc L. Serre^{†,*}

[†]Department of Environmental Sciences and Engineering, Gillings School of Global Public Health, University of North Carolina, Chapel Hill, North Carolina 27599, United States

[‡]Bay Area Air Quality Management District, San Francisco, California 94105, United States

[§]Air Quality Research Center, University of California, Davis, Davis, California 95616, United States

^{||}Pacific Northwest Research Station, United States Department of Agriculture Forest Service, Seattle, Washington 98103, United States

Abstract

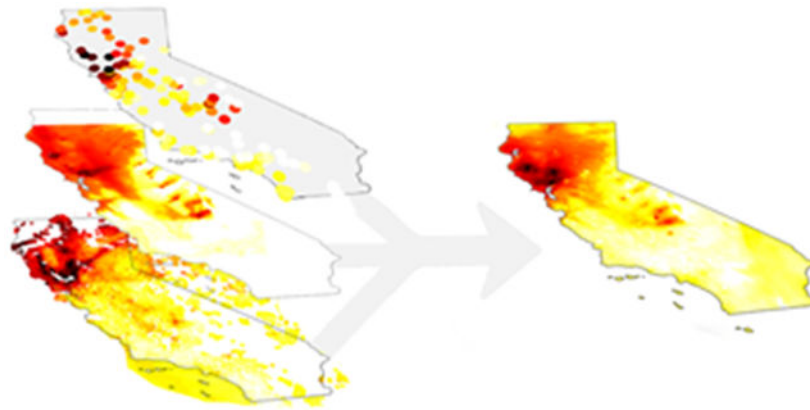
Exposure to wildfire smoke causes adverse health outcomes, suggesting the importance of accurately estimating smoke concentrations. Geostatistical methods can combine observed, modeled, and satellite-derived concentrations to produce accurate estimates. Here we estimate daily average ground-level PM_{2.5} concentrations at a 1-km resolution during the October 2017 California wildfires, using the Constant Air Quality Model Performance (CAMP) and Bayesian Maximum Entropy (BME) methods to bias-correct and fuse three concentration datasets: permanent and temporary monitoring stations, a chemical transport model (CTM), and satellite-derived estimates. Four BME space/time kriging and data fusion methods were evaluated. All BME methods produce more accurate estimates than the standalone CTM and satellite products. Adding temporary station data increases the R² by 36%. The data fusion of observations with the CAMP-corrected CTM and satellite-derived concentrations provides the best estimate (R²=0.713) in fire-impacted regions, emphasizing the importance of combining multiple datasets. We estimate that approximately 65,000 people were exposed to very unhealthy air (daily average PM_{2.5} 150.5 μg/m³).

Graphical Abstract

*Corresponding Author: marc_serre@unc.edu; phone: (919) 966-7014.

The authors declare no competing financial interest.

Supporting Information. Location of PM_{2.5} monitoring stations; AOD to PM_{2.5} conversion; CAMP correction figures; additional details on BME; covariance of PM_{2.5} data; additional details on global offsets; equations used for performance evaluation; state-wide all-month performance statistics; refinement of plume shape with addition of temporary data; stratified performance statistics with the addition of temporary data; further comparison of BME methods; animation of estimated PM_{2.5} concentrations; variance maps of estimated PM_{2.5} concentrations. This information is available free of charge via the Internet at <https://pubs.acs.org/doi/10.1021/acs.est.0c03761>.



Introduction

On October 8-9, 2017, wildfires started in northern California, burning for multiple weeks and spreading over nine counties. During the fires, more than 230,000 acres burnt, nearly 9,000 buildings were destroyed, and 43 people died¹. Wildfires produce emissions that adversely impact air quality, and in turn, human health²⁻⁴. Of wildfire emissions, particulate matter (PM) poses the biggest risk to public health, with fine particles 2.5 μm or smaller ($\text{PM}_{2.5}$) causing the greatest health concern⁵. During the October 2017 fires, $\text{PM}_{2.5}$ concentrations reached the highest levels recorded until that date in the Bay Area, exposing a large population to unhealthy air⁶. Given the potentially severe health impacts of smoke exposure and the likely increase in the frequency, intensity, and spread of wildfires due to climate change⁷⁻¹⁰, it is important to estimate wildfire smoke concentrations to better estimate population exposure, identify at-risk populations, characterize the risk of adverse health outcomes, and inform policy and decision-making processes.

Population-level exposure to wildfire emissions is typically estimated using one or more primary datasets: monitoring station observations, chemical transport models (CTMs), and satellite-based measurements^{11,12}. Each dataset has strengths and weaknesses for estimating wildfire $\text{PM}_{2.5}$ concentrations. Monitoring station observations provide high-quality, accurate measurements that are readily available, but these observations are limited to fixed locations which restricts the ability to understand smoke plume size and location, a significant gap given the rapid change in smoke concentrations over short distances. CTMs, on the other hand, can incorporate knowledge of emissions, atmospheric physics and chemistry, and meteorological conditions to predict $\text{PM}_{2.5}$ at a fine space/time (s/t) resolution, but CTMs have biases and depend upon fire emissions estimates, which have large uncertainty¹³. Satellite observations provide high s/t coverage and valuable information on smoke plume size and location, but do not directly measure $\text{PM}_{2.5}$. Instead $\text{PM}_{2.5}$ is estimated from aerosol optical depth (AOD) measurements and the conversion to ground-level $\text{PM}_{2.5}$ can impact accuracy¹⁴, especially since AOD measurements do not resolve the vertical distribution of smoke plumes. AOD observations are also limited by cloud cover. While these datasets are often used independently for smoke exposure estimates, geostatistical methods can combine observations with modeled and satellite-derived concentrations to produce more accurate estimates during a fire. Previous studies

have found that combining multiple PM_{2.5} datasets, through data fusion, regression modeling, and machine learning methods, often leads to improvements in wildfire PM_{2.5} estimations, compared to using just one dataset^{12,15–20}.

While the benefits of combining these datasets has been shown, to our knowledge, no prior study has evaluated the accuracy of fusing observations from both permanent and temporary monitoring stations with bias-corrected CTM and satellite-derived concentrations to estimate daily average wildfire PM_{2.5}. This study aims to evaluate the accuracy of using the Constant Air Quality Model Performance (CAMP) method in combination with the Bayesian Maximum Entropy (BME) framework to estimate daily average ground-level PM_{2.5} concentrations during the October 2017 wildfires by bias-correcting CTM concentrations and fusing them with monitoring station observations and satellite-derived estimates. The BME framework is an established tool for predictive s/t mapping²¹ that produces accurate s/t concentration estimates and associated measures of uncertainty at unmonitored locations²². Previous studies have used BME to estimate PM_{2.5} in the United States (US)^{23–26}, but it has never been applied to a wildfire event. Additionally, while previous studies have used CAMP to bias-correct modeled PM_{2.5} across the US²⁷, this is the first time it has been implemented to account for the non-linear heteroscedastic bias present in CTM concentrations during a fire. We evaluate the accuracy of four different BME s/t kriging and data fusion methods to identify which BME methods and combination of PM_{2.5} datasets best estimate ground-level PM_{2.5} concentrations during the October 2017 wildfires. Our findings can be used to improve air quality evaluation, management, and prediction during wildfires and characterize population smoke exposure and health risk.

Methods

Study Area and Period.

We estimated daily average ground-level PM_{2.5} concentrations at a 1-km resolution over California, October 1–31, 2017, with the fire period defined as October 8–20 and the fire-affected region defined as California north of 36° latitude. While our analyses focused on estimating concentrations within the fire period and region, we estimated daily average PM_{2.5} for all of October across California in order to understand concentrations more broadly.

Monitoring Station Data.

Daily average PM_{2.5} observations were obtained from permanent Federal Reference Methods (FRM) and Federal Equivalent Methods (FEM) monitoring stations and temporary non-FRM/FEM monitoring stations. The FRM/FEM daily average observations were downloaded from the US Environmental Protection Agency (EPA)'s Air Quality System database (<https://www.epa.gov/aqs>) between October 1–31. The temporary monitoring stations were deployed by the California Air Resources Board (CARB) and data were obtained from the US Forest Service (USFS) who aggregate the data as part of the interagency Wildland Fire Air Quality Response Program (WFAQRP)²⁸. CARB and the WFAQRP place temporary stations in impacted regions to monitor air quality during wildfires. The temporary stations are Met One Instruments, Inc. Environmental Beta

Attenuation Monitors (E-BAM) and E-Samplers monitors, which are designed to accurately predict FRM/FEM PM measurements but are not approved for PM_{2.5} compliance monitoring. We averaged hourly concentrations from the temporary stations to obtain daily averages. In total, observations from 114 FRM/FEM and 49 temporary monitoring stations across California were used (supporting information). Both datasets were cleaned by removing observations less than or equal to zero or with incomplete s/t coordinates, and by averaging concentrations at monitors with duplicate s/t coordinates. The PM_{2.5} observations, and the CTM and satellite-derived concentrations described below, were natural log-transformed prior to use given their lognormal distribution.

Community Multiscale Air Quality Model Data.

The Community Multiscale Air Quality (CMAQ)²⁹ simulations, conducted by the Bay Area Air Quality Management District (BAAQMD), provided estimates of daily average pollutant concentrations in the central California region at a 4-km resolution for October 3-20. Fire emissions estimates for CMAQ were processed using the Fire Detection and Characterization (FDC)³⁰ products from the GOES-16 geostationary satellite, the National Aeronautics and Space Administration (NASA) Fire Energetics and Emissions Research (FEER)³¹ algorithm, and the Sofiev algorithm for plume rise³². The combined high temporal resolution of the FDC product (5-min) coupled with the improved spatial resolution (2-km at nadir) than older generation geostationary satellites, allowed us to simulate the overnight and early morning ignition and large fire activity of October 8–9 that would otherwise been missed using default approaches²⁹. In addition to fire emissions, CMAQ was run with emissions from all other natural and anthropogenic sources, using the CARB's emission inventory for area and nonroad sources, EMFAC2017 model output for on-road sources, EPA BEIS3.61 model output for biogenic sources, and BAAQMD's facility-level emissions data for point sources.

AOD Data.

AOD observations from the Moderate Resolution Imaging Spectroradiometer (MODIS) Terra Satellite were used to obtain AOD-derived PM_{2.5} estimates. The 3-km resolution AOD data (MOD04_3K) using the Collection 6 Dark Target (DT) aerosol algorithm were downloaded from the Level-1 and Atmosphere Archive and Distribution System Distributed Active Archive Center (<https://ladsweb.nascom.nasa.gov/>) for October 1-31. MODIS-retrieved AOD is frequently used to estimate PM_{2.5} at both local and global scales³³.

Conversion of AOD to PM_{2.5}.

To convert the MODIS AOD observations into PM_{2.5} concentrations, we used a mixed effects model (MEM)^{14,34}. Only valid, non-negative AOD observations were used. First, collocated PM_{2.5} and AOD observations were paired, where daily average PM_{2.5} observations were matched with AOD observations when the station location was within the 3-km grid cell on the same day as the satellite overpass. During October 2017, all overpass times occurred between 9 AM and 1 PM local time. Once paired, we fit a day-specific linear MEM to 75% of the matched data and used the remaining 25% to validate (supporting information). Our MEM created a varying intercept and slope for each day, allowing for day-to-day variability in the AOD-PM_{2.5} relationship³⁴ and can be described as

$$PM_{2.5ij} = (\beta_0 + u_{0j}) + (\beta_1 + u_{1j}) \times AOD_{ij} + \varepsilon_{ij} \quad (1)$$

where $PM_{2.5ij}$ is the $PM_{2.5}$ concentration at location i on day j , AOD_{ij} is the collocated AOD measurement, β_0 and β_1 are the fixed intercept and slope, respectively, u_{0j} and u_{1j} are the day-specific random intercept and slope, respectively, and ε_{ij} is the error term at location i on day j . The MEM was then applied to all AOD observations in California during October 2017 to produce estimates of $PM_{2.5}$ and associated variance. The final satellite-derived output (Sat- $PM_{2.5}$) had an R^2 of 0.323 in the fire-affected region and period and was incorporated in the BME framework as soft data, described below.

CAMP Method.

The CAMP method was implemented to bias-correct the CMAQ log- $PM_{2.5}$ concentrations^{27,35}. CAMP corrects for bias differentially over the range of values estimated, for example, by providing a larger bias correction for high estimates than for low estimates. The CAMP method corrects modeled concentrations by modeling the mean and variance of the observed value as a function of the modeled value, accounting for the non-linear and non-homoscedastic relationship between the two. CAMP does this by first pairing collocated modeled concentrations with observations. These paired values are divided into decile bins and the mean (λ_1) and variance (λ_2) of observed log-concentrations in each bin are calculated as

$$\lambda_1(\tilde{y}_i) = \frac{1}{n(\tilde{y}_i)} \sum_{j=1}^{n(\tilde{y}_i)} \hat{y}_j \quad (2)$$

$$\lambda_2(\tilde{y}_i) = \frac{1}{n(\tilde{y}_i) - 1} \sum_{j=1}^{n(\tilde{y}_i)} (\hat{y}_j - \lambda_1(\tilde{y}_i))^2 \quad (3)$$

where $n(\tilde{y}_i)$ is the number of paired modeled (\tilde{y}_i) and observed (\hat{y}_j) log- $PM_{2.5}$ values in each decile bin. The $\lambda_1(\tilde{y}_i)$ and $\lambda_2(\tilde{y}_i)$ s are made into piecewise linear functions by connecting the points estimated in each decile bin, which are used to obtain λ_1 and λ_2 for each modeled log-concentration. The CAMP-calculated mean (λ_1) represents the bias-corrected CMAQ log-concentration and the variance (λ_2) represents the accuracy of the bias-corrected value. To account for bias due to uncertainty in the fire emission estimates, two separate CAMP corrections were applied: one to the fire-affected region and period and one to all other regions and days (supporting information). The final combined product is referred to as the CAMP-corrected CMAQ model output (CC-CMAQ) and was incorporated in the BME framework as soft data.

BME Framework.

The BME framework uses modern spatiotemporal geostatistics to estimate daily average $PM_{2.5}$ concentrations at unmonitored locations by fusing together different types of data³⁶⁻³⁸, using the general knowledge base (G-KB) and the site-specific knowledge base (S-KB) which characterize the general characteristics of the pollutant and the uncertainty in

the data, respectively. Further details on the BME theory and its numerical implementation can be found in supporting information and previously published research^{22,23,35,39–42}. In short there are two aspects of BME modeling, as follows:

First, we transform the air pollution data so it can be modeled as a zero-mean homogeneous/stationary space/time random field (S/TRF). We use the letter Z to represent $\text{PM}_{2.5}$, Y to represent $\log\text{-PM}_{2.5}$, X to represent offset-removed $\log\text{-PM}_{2.5}$, and $o_Y(\mathbf{p})$ to denote the global offset capturing the trend of $\log\text{-PM}_{2.5}$ concentrations as a function of s/t location $\mathbf{p} = (s, t)$, where s is a spatial location, and t is time. The transformation consists in removing the global offset from the observed log-transformed concentration data, which we model as the zero-mean homogenous and stationary S/TRF $X(\mathbf{p})$. By adding the offset back to $X(\mathbf{p})$ we obtain

$$Y(\mathbf{p}) = X(\mathbf{p}) + o_Y(\mathbf{p}) \quad (4)$$

which is the S/TRF describing $\log\text{-PM}_{2.5}$ across the domain. Using this representation, the estimate \tilde{y}_k of $\log\text{-PM}_{2.5}$ at an unmonitored location \mathbf{p}_k , is simply obtained by adding $o_Y(\mathbf{p}_k)$ to the BME estimate \tilde{x}_k for $X(\mathbf{p}_k)$.

Second, we obtain \tilde{x}_k by implementing BME on $X(\mathbf{p})$. The G-KB includes the mean and covariance of the offset-removed $\log\text{-PM}_{2.5}$ S/TRF $X(\mathbf{p})$, which we modeled using the observations from FRM/FEM and temporary monitoring stations during October 2017 (supporting information). The S-KB consists of the offset-removed $\log\text{-PM}_{2.5}$ concentrations from monitoring stations and the offset-removed CC-CMAQ and Sat- $\text{PM}_{2.5}$ log-transformed outputs. The S-KB treats concentrations as either hard data or soft data, where hard data have no associated uncertainty while soft data do. The hard data are the offset-removed $\log\text{-PM}_{2.5}$ monitoring station observations. Hard data have the greatest influence on the BME estimation, with each observation's influence decreasing with increased distance from the monitoring site based on the s/t covariance in the G-KB. The soft data are the CC-CMAQ and Sat- $\text{PM}_{2.5}$ offset-removed log-concentrations and their associated uncertainty. The soft data are described by a PDF which is the product of Gaussian distributions with a mean and variance equal to the offset-removed λ_1 (Eq. 2) and λ_2 (Eq. 3) at each CMAQ grid cell point and equal to the offset-removed satellite-derived concentration (Eq. 1) and its associated variance at each satellite grid cell point. Soft data with lower associated uncertainty have greater influence on the BME estimate. When no soft data is used, BME reduces to simple kriging, given the assumption that the offset-removed log-concentrations have a mean of zero.

For this analysis, two s/t global offsets were considered. The first is a separable s/t global offset (SSTO), which is typically used in the BME framework^{22,24,39} and assumes that the global offset is the combination of a purely spatial and purely temporal offset. The SSTO of $\log\text{-PM}_{2.5}$ is calculated by

$$o_Y(\mathbf{p}) = \log(o_s(\mathbf{s}) + o_t(t) - \overline{o_t(t)}) \quad (5)$$

where the spatial global offset, $o_s(s)$, and temporal global offset, $o_t(t)$, of $PM_{2.5}$ are obtained by applying an exponential smoothing function to the time-averaged and spatially-averaged data, respectively⁴³ (supporting information). The second is a composite s/t global offset (CSTO) which assumes that each s/t location has unique trend across space and time⁴⁴. At any s/t location p , the CSTO for $\log-PM_{2.5}$ is calculated by

$$o_Y(p) = \log\left(\frac{\sum_{i=1}^N w_i * \hat{z}_i}{\sum_{i=1}^N w_i}\right) \quad (6)$$

where N is the number of $PM_{2.5}$ observations within a set s/t radius of s/t location p , and w_i is the weight assigned to the measurement. w_i is determined by both the s/t distance between p_i and p and the spatial and temporal ranges of the exponential smoothing function. The SSTO and CSTO used the same spatial and temporal smoothing ranges (supporting information).

We first compared three versions of BME s/t kriging of observations: with and without data from temporary monitoring stations and with a CSTO compared to a SSTO. We then compared four BME estimation methods: BME s/t kriging of observations, where only hard data are used, and three different versions of BME data fusion, using both hard and soft data.

Method Performance Evaluation.

To evaluate the performance of the BME estimation methods, two cross-validation approaches were used to generate performance statistics: a leave-one-out cross-validation (LOOCV) and a radius cross-validation (RCV). In both, FRM/FEM and temporary station observations are considered true values given the accuracy of the E-BAM and E-Samplers. The LOOCV estimates the $\log-PM_{2.5}$ concentration at each observation s/t location, without using knowledge of the observation. The RCV estimates the $\log-PM_{2.5}$ concentration at each observation s/t location, without using knowledge of all observations at and within a defined radius of that location for all time points. For the RCV, nine spatial radiuses are analyzed, $0-4^\circ$ at increments of 0.5. For both cross-validations, we compared the resulting $\log-PM_{2.5}$ estimations to the observations in order to calculate the following performance statistics: mean square error (MSE), R^2 , mean error (ME), variance of error (VE), and variance of estimation (V_Z) (supporting information). The LOOCV performance statistics were also calculated for the satellite-derived and CTM concentrations, as is and CAMP-corrected. For this, model and satellite-derived values were compared to observations from the same day and located within the model or satellite grid cell. All performance statistics were calculated for October 8-20 in northern California to understand performance in the fire-affected region and period. Performance statistics for October 1-31 across California can be found in supporting information.

Results and Discussion

Mapping $PM_{2.5}$ Through BME S/T Kriging of Observations.

We first evaluated the accuracy of using BME s/t kriging on observed data to estimate $PM_{2.5}$ in northern California during the wildfires. For this evaluation, the CC-CMAQ and Sat-

PM_{2.5} data were not used and three different BME s/t kriging approaches were compared to identify the most accurate estimation method based on observations only. Doing this also allowed us to understand the added value of temporary monitoring station data and a CSTO.

Overall, BME s/t kriging of both FRM/FEM and temporary station data with a CSTO provides the most accurate estimation in the fire-affected region and period (Table 1) and across California for October 1-31 (supporting information). Adding temporary station data to the BME s/t kriging estimation improves accuracy, with a 40% reduction in MSE and a 36% increase in R², and increases the number of monitoring stations used from 114 to 163 and daily observations from 2,670 to 3,621. The increase in observations in smoke-impacted areas results in a refinement of the smoke plume shape (supporting information). While incorporating the temporary station data does not impact performance at the FRM/FEM sites, it notably improves performance at the temporary station locations (supporting information). Although non-FRM/FEM temporary stations use technology not approved to monitor compliance with air quality standards, which may be less accurate, they provide critical concentration information in unmonitored locations and improve overall estimation accuracy during the fires.

Additionally, implementing a CSTO compared to a SSTO results in a slight increase in estimation accuracy, with a 3% reduction in MSE and a 0.2% increase in R². A SSTO is sufficient when all geographic locations in the study area have the same temporal variation in concentrations, but when this assumption is not met, a CSTO allows each geographic location to have a unique time trend⁴⁴. During the October 2017 wildfires, the assumption of a constant temporal trend in PM_{2.5} across space is not met, with the smoke plume only impacting s/t PM_{2.5} trends at monitoring stations in northern California. Using a CSTO more accurately characterizes the PM_{2.5} spatial and temporal variations during the fires, resulting in a slight increase in precision.

While BME s/t kriging of observations accurately estimates PM_{2.5} during the fires, relying solely on observed data has limitations since the estimates are limited by the locations of the s/t observations. In station-dense regions, BME s/t kriging reliably estimates PM_{2.5}, but in many scenarios, such as the October 2017 wildfires, the regions most impacted by smoke have low monitoring station coverage. This limited coverage can lead to unreliable BME estimates in data-scarce, smoke-impacted regions. Additionally, BME s/t kriging on observations only does not incorporate critical knowledge of meteorological conditions, atmospheric physics and chemistry, and smoke plume shape and location, all of which impact smoke concentrations. This limitation can result in an oversimplification and over-smoothing of the estimation surface. Incorporating CTM and/or satellite-derived outputs into the BME framework has the potential to further refine and improve wildfire PM_{2.5} estimations.

Mapping PM_{2.5} Through BME Data Fusion of Observations, CTM, and Satellite Outputs.

To account for non-linear heteroscedastic bias prior to BME data fusion, the CMAQ output was CAMP-corrected. CAMP-correcting the modeled concentrations improves accuracy, with a 9% increase in R² and a 53% reduction in MSE (Table 2). When compared to Sat-

PM_{2.5}, CC-CMAQ provides more accurate PM_{2.5} estimations, with a lower MSE and higher R².

We next compared four BME approaches using the three data sources: observations, CTM output, and satellite-derived estimates. The four BME approaches compared were: BME s/t kriging of observations; BME data fusion of observations and CC-CMAQ; BME data fusion of observations and Sat-PM_{2.5}; and BME data fusion of observations, CC-CMAQ, and Sat-PM_{2.5}. All methods used temporary monitoring station data and a CSTO. Comparing these four methods allowed us to independently evaluate the added value of the CAMP-corrected CTM and satellite-derived outputs in northern California during the wildfires.

The LOOCV results show that all four BME approaches outperform the standalone CC-CMAQ and Sat-PM_{2.5} outputs, with lower MSE and higher R² values (Table 2). Of the four methods, the BME data fusion of observations with CC-CMAQ and Sat-PM_{2.5} is most accurate in the fire-affected region and period, with the lowest MSE and highest R². Of the four BME methods, BME s/t kriging of observations performs worst, with the BME data fusion of all three datasets providing a 3% reduction in MSE and a 1% increase in R². The BME data fusions of observations with CC-CMAQ and Sat-PM_{2.5} and with just CC-CMAQ have the lowest bias and random error. All three BME data fusion methods tend to underestimate the true value while BME s/t kriging tends to overestimate.

While LOOCV is a good assessment of performance, it only evaluates the method's ability to estimate concentrations at monitoring station locations, which may not be located in fire-affected regions. We analyzed the RCV results to identify the most accurate BME method in station-scarce, smoke-impacted regions (Figure 1). Aligning with the LOOCV results, the BME data fusion of observations, CC-CMAQ, and Sat-PM_{2.5} performs best, with the lowest MSE and highest R² at greater distances from the nearest station. The BME data fusion of observations with CC-CMAQ performs similarly, but slightly worse, in comparison. BME s/t kriging of observations performs worst. Once an estimation location is more than 0.5° from the closest station, the BME data fusions of observations with CC-CMAQ and Sat-PM_{2.5} and with just CC-CMAQ perform notably better than the BME data fusion of observations with Sat-PM_{2.5} and BME s/t kriging of observations. State-wide performance statistics for October 1-31 show slightly better LOOCV and worse RCV results compared to the fire-affected region and period, with BME s/t kriging and the BME data fusion of all three performing best in station-dense and station-scarce regions, respectively (supporting information).

We next compared the four BME methods visually to identify physical differences in the estimation surfaces. Maps of each BME method for October 10 (Figure 2) reveal similar PM_{2.5} estimations across California, with a plume of high concentrations north of the Bay Area. The primary difference between the estimation surfaces is the smoke plume shape refinement that occurs once the observations are fused with the CC-CMAQ and/or Sat-PM_{2.5} output. While CC-CMAQ and Sat-PM_{2.5} provide different refinements, incorporating either avoids over-smoothing the estimation surface, which occurs when kriging observations. When both CC-CMAQ and Sat-PM_{2.5} are incorporated into the BME estimation, there is the added benefit of including all available smoke plume information to produce the most

informed estimate. Maps further highlighting the differences between BME methods can be found in supporting information.

Impact of Wildfire Smoke on PM_{2.5} Concentrations.

The estimation maps of ground-level PM_{2.5} during the fires show daily average concentrations exceeding 190 µg/m³ north of San Francisco Bay (Figure 3), with the highest concentrations occurring on October 10, 11, and 13. The 1-km resolution captures the fine-scale spatial variability of concentrations during the fires, since 1 km (approximately 0.01°) is significantly less than the spatial ranges of the covariance model (supporting information). The EPA identifies 24-hour average PM_{2.5} concentrations greater than 150.5 µg/m³ as very unhealthy, with adverse health impacts seen in both sensitive groups and the general public⁴⁵. When our PM_{2.5} estimates are combined with census tract-level population data, we estimate that 65,466 individuals were exposed to daily average PM_{2.5} greater than 150.5 µg/m³ during the fires, with 64,030 exposed on October 13 alone. Additionally, we estimate that 16 million people on at least one day were exposed to daily average concentrations greater than 35 µg/m³, the EPA's 24-hour PM_{2.5} standard⁴⁶ and the level at which concentrations are unhealthy for sensitive groups⁴⁵. Napa and Sonoma counties were disproportionately impacted by the unhealthy air quality. An animation of the PM_{2.5} estimations during the fires along with maps of the estimation variance for October 8-13 can be found in supporting information.

Discussion.

Our results show that the BME framework, used in combination with the CAMP correction method, can be used to accurately estimate ground-level PM_{2.5} concentrations during a wildfire. All four BME s/t kriging and data fusion methods outperform the standalone CMAQ and satellite-derived products, emphasizing the importance of combining multiple data sources.

Using temporary monitoring station data in addition to FRM/FEM station data has added benefit for estimating PM_{2.5} during a wildfire, increasing the s/t coverage in otherwise data-scarce regions. When available, we recommend including temporary station data in future efforts to estimate wildfire PM_{2.5} concentrations. In our implementation of the BME framework, we treat the temporary station observations as hard data, given the accuracy of the E-BAM and E-Samplers, but where the non-FRM/FEM technology is less accurate, these observations can also be treated as soft data in the BME framework to account for measurement error. Additionally, we recommend that future efforts to estimate wildfire PM_{2.5} consider using a CSTO instead of the standard SSTO to improve accuracy, given the CSTO's ability to characterize the unique spatial and temporal variations in smoke concentrations.

Since CTMs are often relied on for smoke concentration estimates, our results emphasize the importance of bias-correcting CTM output, via the CAMP method, to improve accuracy by accounting for the non-linear and non-homoscedastic relationship between modeled and observed wildfire PM_{2.5}. Combining the CAMP-corrected CTM with observations through BME data fusion further improves estimation accuracy by using observed data and

accounting for the CTM's uncertainty. When a CTM simulation is not available, our cross-validations demonstrate that the BME data fusion of observations with satellite-derived estimates produces similarly accurate ground-level smoke concentration estimates, especially within 0.5° of a monitoring station.

Our results also demonstrate that BME s/t kriging of observations does a poor job of estimating concentrations in fire-affected regions, given that monitoring stations are often located in urban or densely populated areas. If the smoke-impacted region is in a station-scarce area, BME s/t kriging of observations will be inaccurate, and the BME data fusion of observations with bias-corrected CTM and/or satellite-derived concentrations will likely better estimate ground-level concentrations. When possible, it is best to combine all three datasets to produce the most accurate and informed wildfire PM_{2.5} estimates. Further, during wildfires, factors such as wind, topography, and meteorological conditions influence the smoke plume trajectory, leading to non-homogenous concentrations across a region⁴⁷. CTMs account for these factors and when combined with satellite-derived information on smoke plume size and location, it is possible to capture important plume features that are challenging to capture with monitoring stations alone. Incorporating both datasets into the BME framework will likely produce more physically meaningful, heterogeneous ground-level PM_{2.5} estimations during a wildfire, with increased accuracy in both station-dense and station-scarce regions.

While our findings show the importance of combining all three datasets, the contribution of the satellite-derived estimates is likely limited by the AOD to PM_{2.5} conversion. In comparison to CC-CMAQ, Sat-PM_{2.5} had lower accuracy, likely a result of the MEM used. It is possible that a more complex conversion that accounts for factors such as meteorological conditions and land use could improve performance and further increase the added value of the satellite-derived PM_{2.5}. Additionally, the MODIS DT aerosol algorithm has higher errors over urban and non-vegetated surfaces³³, which is common in California; using other satellite AOD products in combination with MODIS AOD may provide improved PM_{2.5} estimates in these areas.

By comparing four different BME methods using three PM_{2.5} datasets, we show that the BME data fusion of all three datasets, observations, CC-CMAQ, and Sat-PM_{2.5}, provides the best estimate of smoke concentrations in fire-affected regions during the October 2017 California wildfires. Further, the 1-km resolution of the BME estimations captures the fine-scale spatial variability of concentrations and allows for the accurate assessment of local-level exposure. In addition to the benefits discussed above, incorporating the CMAQ model into the BME framework allows us to estimate the portion of concentrations attributable to the fires. This feature in combination with the framework's ability to produce measures of uncertainty make the BME data fusion of observations with bias-corrected CTM and satellite-derived concentrations ideal for characterizing the health risk associated with wildfire smoke exposure. Our future work includes using these estimated ground-level PM_{2.5} concentrations to quantify the acute health impacts of smoke exposure during the wildfires.

Supplementary Material

Refer to Web version on PubMed Central for supplementary material.

ACKNOWLEDGEMENTS

The authors would like to acknowledge the NASA Health and Air Quality Applied Sciences Team (Grant #NNX16AQ30G, #NNH16AD18I) and the National Institute of Occupational Safety and Health (T42-OH008673) for funding this research.

REFERENCES

- (1). Porter TW; Crowfoot W; Newsom G 2017 Wildfire Activity Statistics: California Department of Forestry and Fire Protection; 2019.
- (2). Liu JC; Pereira G; Uhl SA; Bravo MA; Bell ML A Systematic Review of the Physical Health Impacts from Non-Occupational Exposure to Wildfire Smoke. *Environ. Res* 2015, 136, 120–132, 10.1016/j.envres.2014.10.015. [PubMed: 25460628]
- (3). Reid CE; Brauer M; Johnston FH; Jerrett M; Balme JR; Elliott CT Critical Review of Health Impacts of Wildfire Smoke Exposure. *Environ. Health Perspect* 2016, 124 (9), 1334–1343, 10.1289/ehp.1409277. [PubMed: 27082891]
- (4). Jaffe DA; O'Neill SM; Larkin NK; Holder AL; Peterson DL; Halofsky JE; Rappold AG Wildfire and Prescribed Burning Impacts on Air Quality in the United States. *J. Air Waste Manage. Assoc* 2020, 10.1080/10962247.2020.1749731.
- (5). Valavanidis A; Fiotakis K; Vlachogianni T Airborne Particulate Matter and Human Health: Toxicological Assessment and Importance of Size and Composition of Particles for Oxidative Damage and Carcinogenic Mechanisms. *J. Environ. Sci. Heal* 2008, 26 (4), 339–362, 10.1080/10590500802494538.
- (6). Bay Area Air Quality Management District. Annual Bay Area Air Quality Summaries <https://www.baaqmd.gov/about-air-quality/air-quality-summaries>. (accessed 1/23/2020).
- (7). Spracklen DV; Mickley LJ; Logan JA; Hudman RC; Yevich R; Flannigan MD; Westerling AL Impacts of Climate Change from 2000 to 2050 on Wildfire Activity and Carbonaceous Aerosol Concentrations in the Western United States. *J. Geophys. Res.* 2009, 114 (D20), 10.1029/2008jd010966.
- (8). Yue X; Mickley LJ; Logan JA; Kaplan JO Ensemble Projections of Wildfire Activity and Carbonaceous Aerosol Concentrations over the Western United States in the Mid-21st Century. *Atmos. Environ.* 2013, 77, 767–780, 10.1016/j.atmosenv.2013.06.003.
- (9). Boegelsack N; Withey J; O'Sullivan G; McMartin D A Critical Examination of the Relationship between Wildfires and Climate Change with Consideration of the Human Impact. *J. Environ. Prot* 2018, 09 (05), 461–467, 10.4236/jep.2018.95028.
- (10). Liu JC; Mickley LJ; Sulprizio MP; Dominici F; Yue X; Ebisu K; Anderson GB; Khan RFA; Bravo MA; Bell ML Particulate Air Pollution from Wildfires in the Western US under Climate Change. *Clim. Change* 2016, 138 (3–4), 655–666, 10.1007/s10584-016-1762-6. [PubMed: 28642628]
- (11). Koman PD; Billmire M; Baker KR; de Majo R; Anderson FJ; Hoshiko S; Thelen BJ; French NHF Mapping Modeled Exposure of Wildland Fire Smoke for Human Health Studies in California. *Atmosphere* 2019, 10 (6), 10.3390/atmos10060308.
- (12). Lassman W; Ford B; Gan RW; Pfister G; Magzamen S; Fischer EV; Pierce JR Spatial and Temporal Estimates of Population Exposure to Wildfire Smoke during the Washington State 2012 Wildfire Season Using Blended Model, Satellite, and in Situ Data. *GeoHealth* 2017, 1 (3), 106–121, 10.1002/2017GH000049. [PubMed: 32158985]
- (13). Larkin NK; Raffuse SM; Strand TM Wildland Fire Emissions, Carbon, and Climate: U.S. Emissions Inventories. *For. Ecol. Manage* 2014, 317, 61–69, 10.1016/j.foreco.2013.09.012.

- (14). Chu Y; Liu Y; Li X; Liu Z; Lu H; Lu Y; Mao Z; Chen X; Li N; Ren M; Liu F; Tian L; Zhu Z; Xiang H A Review on Predicting Ground PM_{2.5} Concentration Using Satellite Aerosol Optical Depth. *Atmosphere*. 2016, 7 (10), 129, 10.3390/atmos7100129..
- (15). Reid CE; Jerrett M; Petersen ML; Pfister GG; Morefield PE; Tager IB; Raffuse SM; Balmes JR Spatiotemporal Prediction of Fine Particulate Matter during the 2008 Northern California Wildfires Using Machine Learning. *Environ. Sci. Technol* 2015, 49 (6), 3887–3896, 10.1021/es505846r. [PubMed: 25648639]
- (16). Yao J; Henderson SB An Empirical Model to Estimate Daily Forest Fire Smoke Exposure over a Large Geographic Area Using Air Quality, Meteorological, and Remote Sensing Data. *J. Expo. Sci. Environ. Epidemiol* 2014, 24 (3), 328–335, 10.1038/jes.2013.87. [PubMed: 24301352]
- (17). Zou Y; O'Neill SM; Larkin NK; Alvarado EC; Solomon R; Mass C; Liu Y; Odman MT; Shen H Machine Learning-Based Integration of High-Resolution Wildfire Smoke Simulations and Observations for Regional Health Impact Assessment. *Int. J. Environ. Res. Public Health* 2019, 16 (12), 2137, 10.3390/ijerph16122137.
- (18). Geng G; Murray NL; Tong D; Fu JS; Hu X; Lee P; Meng X; Chang HH; Liu Y Satellite-Based Daily PM_{2.5} Estimates During Fire Seasons in Colorado. *J. Geophys. Res. Atmos* 2018, 123 (15), 8159–8171, 10.1029/2018JD028573. [PubMed: 31289705]
- (19). Bi J; Wildani A; Chang HH; Liu Y Incorporating Low-Cost Sensor Measurements into High-Resolution PM_{2.5} Modeling at a Large Spatial Scale. *Environ. Sci. Technol* 2020, 54 (4), 2152–2162, 10.1021/acs.est.9b06046. [PubMed: 31927908]
- (20). O'Dell K; Ford B; Fischer EV; Pierce JR Contribution of Wildland-Fire Smoke to US PM 2.5 and Its Influence on Recent Trends. *Environ. Sci. Technol* 2019, 53 (4), 1797–1804, 10.1021/acs.est.8b05430. [PubMed: 30681842]
- (21). He J; Kolovos A Bayesian Maximum Entropy Approach and Its Applications: A Review. *Stoch. Environ. Res. Risk Assess* 2018, 32 (4), 859–877, 10.1007/s00477-017-1419-7.
- (22). Christakos G; Serre ML BME Analysis of Spatiotemporal Particulate Matter Distributions in North Carolina. *Atmos. Environ* 2000, 34 (20), 3393–3406, 10.1016/S1352-2310(00)00080-7.
- (23). Reyes JM; Serre ML An LUR/BME Framework to Estimate PM_{2.5} Explained by on Road Mobile and Stationary Sources. *Environ. Sci. Technol* 2014, 48 (3), 1736–1744, 10.1021/es4040528. [PubMed: 24387222]
- (24). Akita Y; Chen JC; Serre ML The Moving-Window Bayesian Maximum Entropy Framework: Estimation of PM 2.5 Yearly Average Concentration across the Contiguous United States. *J. Expo. Sci. Environ. Epidemiol* 2012, 22 (5), 496–501, 10.1038/jes.2012.57. [PubMed: 22739679]
- (25). Jerrett M; Turner MC; Beckerman BS; Pope CA; van Donkelaar A; Martin RV; Serre M; Crouse D; Gapstur SM; Krewski D; Diver WR; Coogan PF; Thurston GD; Burnett RT Comparing the Health Effects of Ambient Particulate Matter Estimated Using Ground-Based versus Remote Sensing Exposure Estimates. *Environ. Health Perspect*. 2017, 125 (4), 552–559, 10.1289/EHP575. [PubMed: 27611476]
- (26). Beckerman BS; Jerrett M; Serre M; Martin RV; Lee SJ; Van Donkelaar A; Ross Z; Su J; Burnett RT A Hybrid Approach to Estimating National Scale Spatiotemporal Variability of PM_{2.5} in the Contiguous United States. *Environ. Sci. Technol* 2013, 47 (13), 7233–7241, 10.1021/es400039u. [PubMed: 23701364]
- (27). Reyes JM; Xu Y; Vizuete W; Serre ML Regionalized PM_{2.5} Community Multiscale Air Quality Model Performance Evaluation across a Continuous Spatiotemporal Domain. *Atmos. Environ* 2017, 148, 258–265, 10.1016/J.ATMOSENV.2016.10.048.
- (28). United States Congress. S.47 - John D. Dingell, Jr. Conservation, Management, and Recreation Act; 2019.
- (29). Appel KW; Napelenok SL; Foley KM; Pye HOT; Hogrefe C; Luecken DJ; Bash JO; Roselle SJ; Pleim JE; Foroutan H; Hutzell WT; Pouliot GA; Sarwar G; Fahey KM; Gantt B; Gilliam RC; Heath NK; Kang D; Mathur R; Schwede DB; Spero TL; Wong DC; Young JO Description and Evaluation of the Community Multiscale Air Quality (CMAQ) Modeling System Version 5.1. *Geosci. Model Dev* 2017, 10 (4), 1703–1732, 10.5194/gmd-10-1703-2017. [PubMed: 30147852]

- (30). Schmidt CC; Hoffman J; Prins E; Lindstrom S GOES-R Advanced Baseline Imager (ABI) Algorithm Theoretical Basis Document For Fire / Hot Spot Characterization Version 2.6; 2013.
- (31). Ichoku C; Ellison L Global Top-down Smoke-Aerosol Emissions Estimation Using Satellite Fire Radiative Power Measurements. *Atmos. Chem. Phys* 2014, 14 (13), 6643–6667, 10.5194/acp-14-6643-2014.
- (32). Sofiev M; Ermakova T; Vankevich R Evaluation of the Smoke-Injection Height from Wild-Land Fires Using Remote-Sensing Data. *Atmos. Chem. Phys* 2012, 12 (4), 1995–2006, 10.5194/acp-12-1995-2012.
- (33). Bilal M; Qiu Z; Campbell J; Spak S; Shen X; Nazeer M A New MODIS C6 Dark Target and Deep Blue Merged Aerosol Product on a 3 Km Spatial Grid. *Remote Sens.* 2018, 10 (3), 463, 10.3390/rs10030463.
- (34). Lee HJ; Liu Y; Coull BA; Schwartz J; Koutrakis P A Novel Calibration Approach of MODIS AOD Data to Predict PM_{2.5} Concentrations. *Atmos. Chem. Phys* 2011, 11 (15), 7991–8002, 10.5194/acp-11-7991-2011.
- (35). Nazelle A. de; Arunachalam S; Serre ML. Bayesian Maximum Entropy Integration of Ozone Observations and Model Predictions: An Application for Attainment Demonstration in North Carolina. *Environ. Sci. Technol* 2010, 44 (15), 5707–5713, 10.1021/es100228w. [PubMed: 20590110]
- (36). Christakos G A Bayesian/Maximum-Entropy View to the Spatial Estimation Problem. *Math. Geol* 1990, 22 (7), 763–777, 10.1007/BF00890661.
- (37). Serre ML; Christakos G Modern Geostatistics: Computational BME Analysis in the Light of Uncertain Physical Knowledge - The Equus Beds Study. *Stoch. Environ. Res. Risk Assess* 1999, 13 (1–2), 1–26, 10.1007/s004770050029.
- (38). Christakos G; Bogaert P; Serre ML Temporal GIS : Advanced Functions for Field-Based Applications; 2002.
- (39). Christakos G; Serre ML; Kovitz JL BME Representation of Particulate Matter Distributions in the State of California on the Basis of Uncertain Measurements. *J. Geophys. Res. Atmos* 2001, 106 (D9), 9717–9731, 10.1029/2000JD900780.
- (40). Xu Y; Serre ML; Reyes J; Vizuete W Bayesian Maximum Entropy Integration of Ozone Observations and Model Predictions: A National Application. *Environ. Sci. Technol* 2016, 50 (8), 4393–4400, 10.1021/acs.est.6b00096. [PubMed: 26998937]
- (41). Xu Y; Serre ML; Reyes JM; Vizuete W Impact of Temporal Upscaling and Chemical Transport Model Horizontal Resolution on Reducing Ozone Exposure Misclassification. *Atmos. Environ* 2017, 166, 374–382, 10.1016/j.atmosenv.2017.07.033.
- (42). Serre ML; Christakos G; Lee SJ Soft Data Space/Time Mapping of Coarse Particulate Matter Annual Arithmetic Average Over the U.S. In *geoENV IV — Geostatistics for Environmental Applications*; 2006; pp 115–126, 10.1007/1-4020-2115-1_10.
- (43). Akita Y; Carter G; Serre ML Spatiotemporal Nonattainment Assessment of Surface Water Tetrachloroethylene in New Jersey. *J. Environ. Qual* 2007, 36 (2), 508–520, 10.2134/jeq2005.0426. [PubMed: 17332255]
- (44). Lee S-J; Serre ML; van Donkelaar A; Martin RV; Burnett RT; Jerrett M Comparison of Geostatistical Interpolation and Remote Sensing Techniques for Estimating Long-Term Exposure to Ambient PM_{2.5} Concentrations across the Continental United States. *Environ. Health Perspect* 2012, 120 (12), 1727–1732, 10.1289/ehp.1205006. [PubMed: 23033456]
- (45). Environmental Protection Agency. AQI Breakpoints | EPA Air Quality System https://aqs.epa.gov/aqsweb/documents/codetables/aqi_breakpoints.html. (accessed 1/22/2020).
- (46). Environmental Protection Agency. NAAQS Table | Criteria Air Pollutants <https://www.epa.gov/criteria-air-pollutants/naaqs-table>. (accessed 3/19/2020).
- (47). Goodrick SL; Achtemeier GL; Larkin NK; Liu Y; Strand TM Modelling Smoke Transport from Wildland Fires: A Review. *Int. J. Wildl. Fire* 2013, 22 (1), 83–94, 10.1071/WF11116.

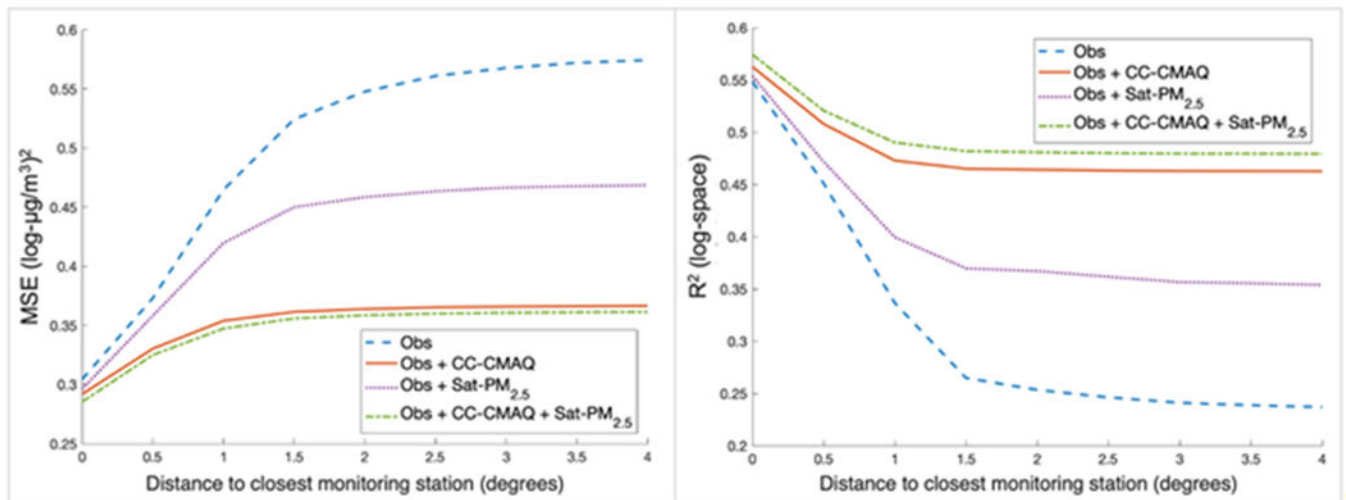


Figure 1. Results of radius cross validation for estimating daily average log-PM_{2.5} in the fire-affected region and period; MSE (left) and R² (right), based on distance to the closest monitoring station, for the 4 BME methods: BME s/t kriging, Observations (Obs); BME Data Fusion, Observations and CC-CMAQ (Obs + CC-CMAQ); BME Data Fusion, Observations and Sat-PM_{2.5} (Obs + Sat-PM_{2.5}); BME Data Fusion, Observations, CC-CMAQ, and Sat-PM_{2.5} (Obs + CC-CMAQ + Sat-PM_{2.5}).

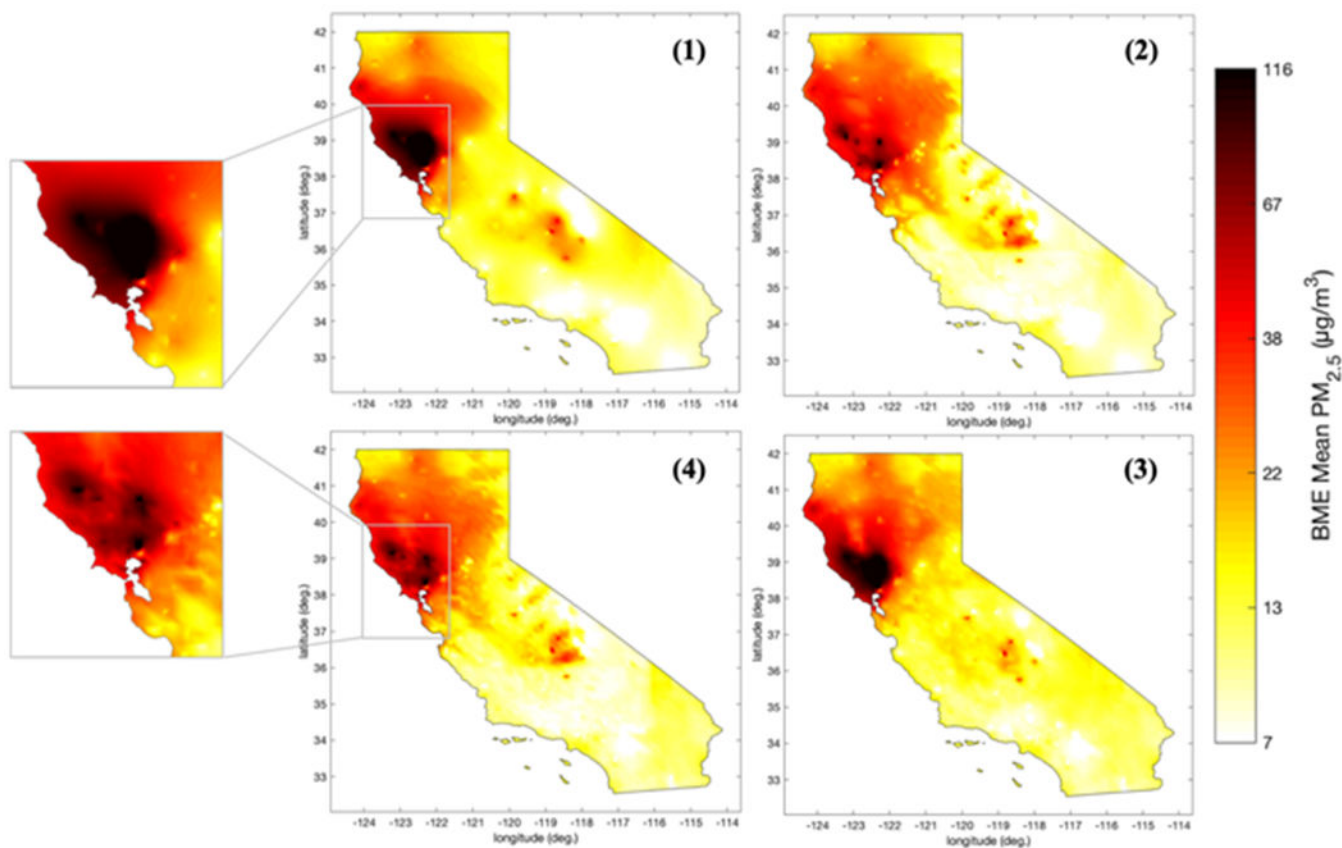


Figure 2. Comparison of 4 BME methods to calculate the median value of daily average $PM_{2.5}$ concentrations on Oct. 10, 2017. (1) BME s/t kriging, Observations; (2) BME Data Fusion, Observations and CC-CMAQ; (3) BME Data Fusion, Observations and Sat- $PM_{2.5}$; (4) BME Data Fusion, Observations, CC-CMAQ, and Sat- $PM_{2.5}$.

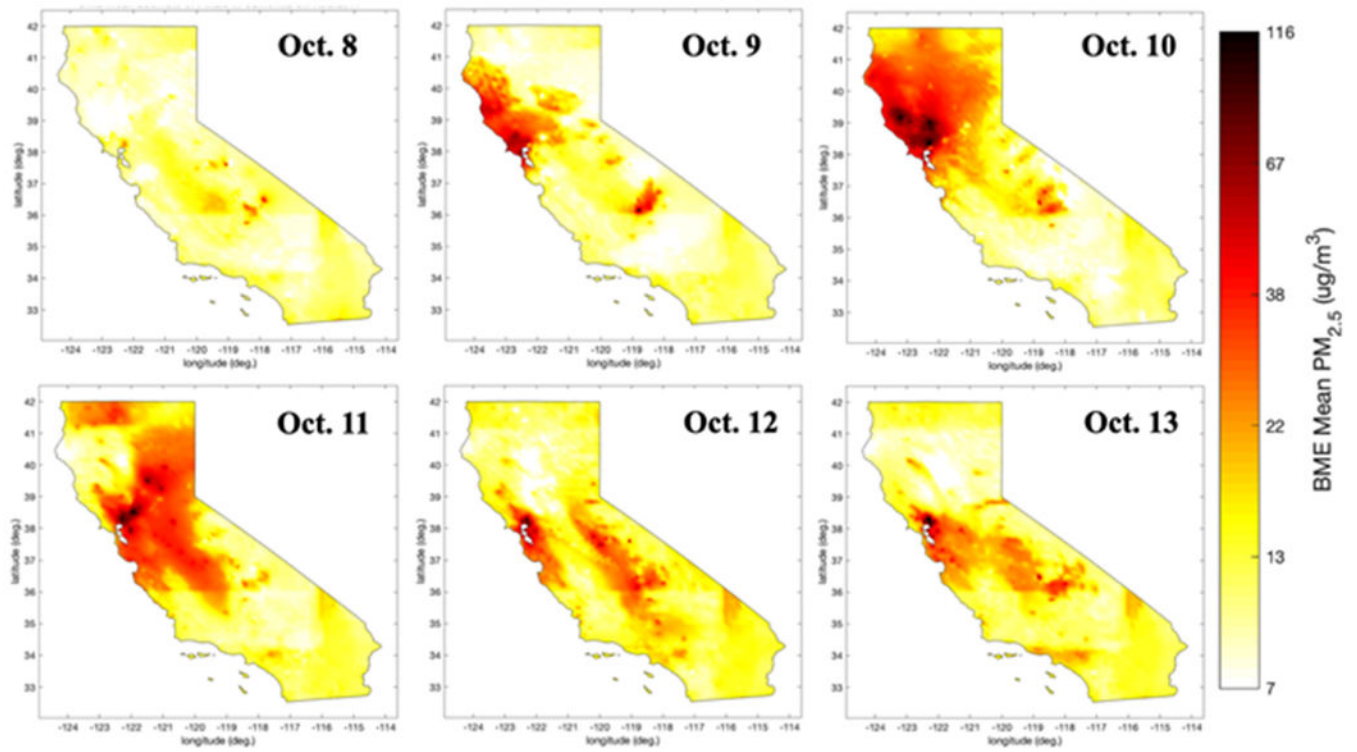


Figure 3. Median value of daily average ground-level PM_{2.5} concentrations, estimated by the BME data fusion of observations, CC-CMAQ, and Sat-PM_{2.5}, across California for Oct. 8-13, 2017.

Table 1.

Leave-one-out cross-validation results for the estimation of the log of PM_{2.5} daily average concentrations in the fire-affected region and period, using three BME s/t kriging approaches.

<i>BME s/t Kriging Method</i>		MSE* (log- μg/m ³) ²	R ² * (log- space)	ME* (log- μg/m ³)	VE* (log- μg/m ³) ²	V _Z * (log- μg/m ³) ²
Observations	Global Offset					
FRM/FEM	Composite	0.327	0.520	-0.096	0.196	0.428
FRM/FEM & Temporary	Separable	0.202	0.706	-0.001	0.202	0.594
FRM/FEM & Temporary	Composite	0.196	0.708	0.003	0.196	0.552

* Performance metrics for the estimation of log-PM_{2.5} include mean square error (MSE), R-squared (R²), mean error (ME), variance of error (VE), and variance of estimation (V_Z). The mean and variance of the observed log-PM_{2.5} data are 2.36 log-μg/m³ and 0.532 (log-μg/m³)², respectively.

Table 2.

Leave-one-out cross-validation results for the estimation of the log of PM_{2.5} daily average concentrations in the fire-affected region and period, using CAMP correction, BME s/t kriging, and BME data fusion approaches.

	MSE * (log- $\mu\text{g}/\text{m}^3$) ²	R ² * (log-space)	ME * (log- $\mu\text{g}/\text{m}^3$)	VE * (log- $\mu\text{g}/\text{m}^3$) ²	V _Z * (log- $\mu\text{g}/\text{m}^3$) ²
Satellite-derived log-PM _{2.5} (Sat-PM _{2.5})	0.365	0.323	0.053	0.362	0.256
CMAQ Model	0.863	0.431	0.226	0.812	1.521
CAMP-Corrected (CC)-CMAQ Model	0.362	0.496	-0.001	0.362	0.375
BME s/t Kriging	0.196	0.708	0.003	0.196	0.552
BME Data Fusion, Observations & CC-CMAQ	0.192	0.709	-0.0001	0.192	0.441
BME Data Fusion, Observations & Sat-PM _{2.5}	0.193	0.708	-0.006	0.193	0.513
BME Data Fusion, Observations, CC-CMAQ, & Sat-PM _{2.5}	0.190	0.713	-0.0003	0.190	0.435

* Performance metrics for the estimation of log-PM_{2.5} include mean square error (MSE), R-squared (R²), mean error (ME), variance of error (VE), and variance of estimation (V_Z). The mean and variance of the observed log-PM_{2.5} data are 2.36 log- $\mu\text{g}/\text{m}^3$ and 0.532 (log- $\mu\text{g}/\text{m}^3$)², respectively.